

Raman anomalies as signatures of pressure induced electronic topological and structural transitions in black phosphorus: Experiments and Theory

Satyendra Nath Gupta¹, Anjali Singh², Koushik Pal², Biswanath Chakraborti¹, D.V.S.Muthu¹, U V Waghmare² and A. K. Sood^{1*}

¹*Department of Physics, Indian Institute of Science, Bangalore-560012, India* ²*Theoretical Sciences Unit,*

Jawaharlal Nehru Centre for Advanced Scientific Research, Bangalore-560064, India

(Dated: November 5, 2018)

We report high pressure Raman experiments of Black phosphorus (BP) up to 24 GPa. The line widths of first order Raman modes A_g^1 , B_{2g} and A_g^2 of the orthorhombic phase show a minimum at 1.1 GPa. Our first-principles density functional analysis reveals that this is associated with the anomalies in electron-phonon coupling at the semiconductor to topological insulator transition through inversion of valence and conduction bands marking a change from trivial to nontrivial electronic topology. The frequencies of B_{2g} and A_g^2 modes become anomalous in the rhombohedral phase at 7.4 GPa, and new modes appearing in the rhombohedral phase show anomalous softening with pressure. This is shown to originate from unusual structural evolution of black phosphorus with pressure, based on first-principles theoretical analysis.

PACS numbers: 78.30.-j, 71.30.+h, 71.15.Mb

I. INTRODUCTION

The Black phosphorus (BP) is the most stable form among the many allotropic modifications of phosphorus at room temperature and ambient pressure. It is an elemental semiconductor with direct band gap of ~ 0.3 eV. Recently there is revival of interest in BP from the prospective of a layered material which allows us to study the exciting properties of a mono and few layers of BP¹⁻⁸. It is found that the band gap depends on the thickness of its film: 0.3eV for thickness $> 4nm$ and 1.2 eV for single layer thick BP⁹. This moderate band gap bridges the gap between the semi-metallic graphene^{10,11} and relatively large band gap of transition metal dichalcogenide (1.5-2.5eV)¹²⁻¹⁴ and makes it ideal for infrared optoelectronic application. Another interesting feature of BP is its anisotropic atomic structure. At ambient pressure, BP packs into orthorhombic lattice with a puckered honeycomb structure as shown in Fig. 1. Each phosphorus atom is bonded with two in-plane and one out of plane neighboring atoms. The puckered layers are bound together by weak van der Waals interactions. Due to this anisotropic atomic structure, the effective masses of carriers in BP along arm chair (ac) are lightest and that along the layer stacking (z) are lighter than that along the zigzag (zz)¹⁵. Recent upsurge of interest in layered BP has arisen due to this unique puckered 2D honeycomb lattice in each phosphorus layer, giving anisotropic electronic⁸, optical^{4,8} and vibrational properties⁴.

Further, the direct band gap ($\sim 0.3eV$) of BP arises from the out-of-plane p_z -like orbitals of phosphorus and hence can be strongly modulated by pressure or c-axis strain. Not surprisingly, the effect of pressure was studied on crystal structure and electronic properties in the early work¹⁶⁻²². It has anisotropic compressibility: lattice parameters a and c decrease more in comparison with the lattice parameter b with increasing pressure. At room

temperature, the ambient pressure orthorhombic structure transforms to the rhombohedral structure at $P_{c2} \sim 4.7$ GPa and then to the simple cubic structure (sc) at $P_{c3} \sim 11$ GPa²². These transition pressures are slightly higher if sample is cooled to liquid helium temperature first and then pressure is increased. The sc phase transforms to a simple hexagonal (sh) phase at higher pressure 137 GPa via an intermediate phase²³. Recently, Akahama et. al²⁴ investigated the crystal structure of black phosphorus up to 280 GPa at room temperature using x-ray-diffraction experiment and found that sh phase goes to the bcc structure at 262 GPa. The sc phase exhibits superconductivity at 4.7 K^{25,26}. The superconducting temperature is slightly pressure dependent and increases with increasing pressure. The superconducting state remains for several hours even if the pressure is removed. BP shows superconductivity with high transition temperature (10K) when it is cooled to 4K first and then pressure is applied. These experiments clearly establish that high pressure can be used to tune the material characteristic of BP significantly.

The electrical conductivity of black P is also very sensitive to pressure²⁷⁻²⁹. Two anomalies have been reported at 1.7 and 4.2 GPa, the latter coinciding with the structural phase transition from orthorhombic to rhombohedral structure. The earlier work³⁰ reported that the band gap decreased linearly with a pressure coefficient of ~ 0.17 eV/ GPa, closing at $P_{c1} \sim 1.5$ GPa. Recent magneto-resistance studies³¹ have termed this transition as electronic topological transition (ETT) from semiconductor to 3D Dirac semi-metal due to band crossover near the Z-point in the Brillouin zone with linear dispersion. Interestingly, a colossal magneto-resistance of $\sim 80,000$ is seen at 2GPa at a field of 9T, similar to 2D Weyl semi-metals like WTe₂, making BP as an elemental semi-metal with increased electronic structure.

Pressure and strain have been used to change the rela-

tive strength of spin-orbit coupling and induce electronic topological transition (ETT) in materials like Sb_2Se_3 ³², $\text{b-As}_2\text{Te}_3$ ³³, BiTeI ³⁴. Recently, Gong *et al.*³⁰ theoretically reported a pressure-induced Lifshitz transition at a pressure of 1.2 GPa where black phosphorus undergoes a semiconductor to three-dimensional Dirac semimetal transition. By using first-principles density functional theoretical calculations within GGA and mBJ exchange-correlation functional, Gong *et al.*³⁰ showed that the band inversion occurs at the Z point at 1.2 GPa and robust three-dimensional Dirac points appear away from the Z point. Recently a theoretical study by Manjanath *et al.*³⁵ reported a reversible semiconductor to metal transition in bilayer phosphorene by applying normal compressive strain. In another work, Xiang *et al.*^{31,36} reported colossal positive magneto-resistance in black phosphorus for $P \geq 1.2$ GPa and observed a non-trivial π Berry phase from the Shubnikov-de Haas oscillation measurement. These observed changes in black phosphorus at pressure of 1.2 GPa were attributed to an electronic Lifshitz transition³¹.

The role of lattice in pressure-induced electronic topological transition has been evident in softening of an acoustic phonon mode at 1.54 GPa in an earlier inelastic neutron scattering experiment³⁷, where anomalous compressibility and softening of longitudinal ultrasonic wave propagating along *c*-axis hint the relevance of electron-phonon interaction to pressure induced transitions. High pressure Raman spectroscopy, a sensitive probe of lattice distortion under pressure, has been used in BP up to 13 GPa pressure, displaying changes in the pressure coefficients of Raman frequencies of a few modes as well as appearance of new modes at the structural transitions at $P_{c2} \sim 4.7$ GPa and $P_{c3} \sim 10.5$ GPa²². Recently, Sasaki *et al.*³⁸ reported high pressure Raman study on few layers phosphorene and compared the results with bulk BP. It was found that monolayer and bilayer phosphorene show different behavior from the bulk sample. We revisit the high pressure Raman studies in this work with two objectives: (i) to see the Raman signature of electronic topological transition at P_{c1} and (ii) to understand the phonon signatures using first-principles density functional theory (DFT). Our main results are (i) The linewidths of the first order Raman modes go through minimum at the ETT near $P_{c1} \sim 1.1$ GPa; (ii) Pressure dependence of phonon frequencies and appearance of new modes confirm the two structural transitions at $P_{c2} \sim 4.6$ GPa and $P_{c3} \sim 11$ GPa; (iii) The first order modes B_{2g} and A_g^2 show anomalous softening in the rhombohedral phase; (iv) All the three Raman modes of the orthorhombic structure vanish above ~ 11 GPa in the sc phase; (v) The new modes appearing in the rhombohedral phase show anomalous decrease in frequency with increasing pressure up to 24 GPa; (vi) Using first-principles analysis we show that the transition at the lowest pressure is an electronic topological transition to a phase with a strong Z_2 topology, while the anomalies at higher pressure have a structural origin. (vii) The new modes labeled N1, N2

and N3 observed in the rhombohedral phase have been quantitatively analyzed theoretically for the first time, capturing their anomalous softening. The modes N1, N2 and N3 have been assigned to E_g^1 , A_{1g} and E_g^2 modes respectively. The modes N1 and N2 in the sc phase are assigned as X and M point acoustic modes, respectively.

II. EXPERIMENTAL DETAILS

Raman measurements were carried out at room temperature in back scattering configuration with micro-optical system equipped with Horiba 800 spectrometer, Peltier-cooled charge controlled detector and 532 nm diode laser. Pressure was generated using a diamond anvil cell (DAC) using 4:1 methanol: ethanol pressure transmitting medium. A thin platelet of dimension $\sim 100\mu\text{m}$ cleaved from single crystals of BP, (from M/S Smart Elements) was placed into a stainless steel gasket with sample chamber hole of $\sim 200\mu\text{m}$ inserted between the diamonds along with a ruby chip for pressure calibration. Laser power ($< 5\text{mW}$) was kept low enough to avoid damage to the sample.

III. COMPUTATIONAL DETAILS

Our first-principles calculations are based on density functional theory (DFT) as implemented in the Quantum ESPRESSO package³⁹, with the interaction between ionic core and valence electrons modeled with norm-conserving pseudopotentials^{40,41}. The exchange-correlation energy of electrons is treated within a generalized gradient approximation (GGA) with a functional form parameterized by Perdew, Burke and Ernzerhof⁴². We use an energy cutoff of 55 Ry to truncate the plane wave basis used in representing Kohn-Sham wave functions, and energy cutoff of 220 Ry for the basis set to represent charge density. Structures are relaxed to minimize energy till the magnitude of Hellman-Feynman force on each atom is less than $0.03 \text{ eV}/\text{\AA}$. We include van der Waals (vdW) interaction with the parametrization given in Grimme scheme⁴³. In self-consistent Kohn-Sham (KS) calculations of configurations of bulk black phosphorus with orthorhombic and rhombohedral unit cell, the Brillouin zone (BZ) integrations were sampled with a uniform mesh of $18 \times 16 \times 16$ and $16 \times 16 \times 16$ k-points respectively, and $32 \times 32 \times 32$ mesh of k-points was used in calculation of electron-phonon coupling of both the structural forms. Phonon spectra and dynamical matrices at Γ -point ($q=(0, 0, 0)$) as a function of lattice constant (or pressure) were determined using density functional linear response as implemented in Quantum ESPRESSO(QE)³⁹, which employs the Green's function method to avoid explicit calculations of unoccupied Kohn-Sham states. Since DFT typically underestimates the electronic bandgap, we have used HSE functional⁴⁴ to estimate the gaps accurately, with the mixing parameter of 0.25 and reciprocal

space integration sampled on a 4x4x4 mesh of k-points. We have fully relaxed the orthorhombic structure of BP with HSE calculations maintaining the experimental c/a ratio. We find that the error in resulting cell volume (relative to experiments) is negligibly zero (Fig. 2 (a)). Fitting a quadratic function to energy vs. volume curve, we used $-\frac{dE}{dV}$ to estimate pressures within HSE calculations. We determine electronic bandgap at Z-point as a function of volume, and used the point of minimum bandgap to estimate the transition pressure within HSE calculations (Fig. 2 (b)).

Z_2 topological invariants can be defined using the notion of time reversal polarization^{45,46} derived in terms of hybrid Wannier charge centers (WCCs)⁴⁷. In a time-reversal invariant system, electronic bands always come in time-reversed pairs (let's say I & II denote such pairs). Then the Z_2 invariant in a time-reversal invariant plane is given by⁴⁵,

$$\left(\sum_n [\bar{x}_n^I(T/2) - \bar{x}_n^{II}(T/2)] - \sum_n [\bar{x}_n^I(0) - \bar{x}_n^{II}(0)] \right) \text{ mod } 2, \quad (1)$$

where $\bar{x}_n = \frac{i}{2\pi} \int_{-\pi}^{\pi} dk < u_{nk} | \frac{\partial}{\partial k} | u_{nk} >$ is the Wannier charge center calculated at $t=0$ and $t=T/2$ planes which are invariant under time reversal symmetry, where T represents the period of a full cyclic adiabatic evolution. In the Brillouin zone of a periodic crystal T is equivalent to a reciprocal lattice vector which defines the periodicity in the reciprocal space. The topological invariant of a plane is non-zero if the WCCs switch pairs under an adiabatic evolution in the half-cycle, which can be easily tracked by seeing evolution of the mid-point of the largest gap (as marked by blue rhombus in Fig. 9) between two adjacent WCCs with $t \in [0, T/2]$ in the half-cycle⁴⁵. In this case, the rhombuses exhibits abrupt jumps in their half-cyclic evolution and cross odd number of WCCs⁴⁵. We have calculated the strong topological index (ν_0) by taking the sum (modulo 2) of the topological invariants calculated at $k_z=0$ and $k_z=0.5$ planes in the Brillouin zone of black phosphorous using Z2Pack code⁴⁸. At each of these planes, WCC, calculated along k_x direction, evolve along the k_y direction (parameterized with time, t).

IV. RESULTS AND DISCUSSION

A. Experimental Results

The unit cell of BP contains 4 atoms which gives 12 normal modes. According to factor group analysis, at ambient pressure the Brillouin zone center point phonon modes are $2A_g + B_{1g} + B_{2g} + 2B_{3g} + A_u + 2B_{1u} + 2B_{2u} + B_{3u}$: out of which $2A_g$, B_{1g} , B_{2g} and $2B_{3g}$ are Raman active. Experimentally three Raman modes A_g^1 , B_{2g} and A_g^2 were observed at 360, 438 and 460 cm^{-1} respectively as shown in lower panel of Fig. 3. The other two previously reported²² Raman modes B_{1g} (192 cm^{-1}) and B_{3g}^1

(227 cm^{-1}) are very weak and difficult to separate from the background. The phosphorus atoms vibrate along the out of plane (z) for the A_g^1 (360 cm^{-1}) mode, along armchair (y) for the B_{2g} (438 cm^{-1}) mode and zig zag (x) directions for the A_g^2 (460 cm^{-1}) mode. Fig. 3 shows the pressure evolution of the Raman spectra of BP at a few representative pressures. The Lorentzian line shapes are used to fit the Raman spectra at different pressures to obtain phonon frequencies and full width at half maximum (FWHM). From Fig. 3, it can be seen that the intensities of A_g^1 , B_{2g} and A_g^2 Raman modes of the orthorhombic structure decrease gradually with pressure and disappear completely at 11 GPa. Further, two new Raman modes labelled as N1 and N2 at 240 and 300 cm^{-1} respectively, emerged at 4.6 GPa and remain till 24 GPa. Another new mode labelled as N3 at 370 cm^{-1} arises at 7.4 GPa and diminishes at 15.9 GPa. To shed more light on the evolution of modes N1, N2 and N3 with pressure, we examine the frequencies and area of N1, N2 and N3 peaks as a function of pressure (see Fig. 4). It is clear that the intensity of N1 mode increases slowly with increasing pressure till 10 GPa, and rapidly beyond 10 GPa. The intensity of N2 and N3 modes increases with pressure till 13 GPa, and decreases beyond that. The phonon frequencies of N1, N2 and N3 modes soften with pressure.

Fig. 5 shows the pressure dependence of phonon frequencies. The solid blue lines are the linear fit to the experimental data points. The vertical dashed red lines indicate two structural phase transitions from orthorhombic to rhombohedral and from rhombohedral to simple cubic phase. Fig. 5 shows that the frequencies of A_g^1 , B_{2g} and A_g^2 modes show increase with pressure in orthorhombic phase. The slope for the A_g^1 ($S=d\omega/dP$) is more as compared to that for the B_{2g} and A_g^2 modes. Noting that the eigen vectors of the A_g^1 mode are perpendicular to the puckered layers, larger pressure derivative of frequency (S) signifies that van der Waals bond can be greatly compressed. Fig. 5 also shows that all the three modes of the orthorhombic phase (A_g^1 , B_{2g} and A_g^2) persist even beyond 4.6 GPa. This can be due to two possibilities (i) that the orthorhombic to rhombohedral transformation is completed only at ~ 11 GPa; (ii) the Raman active modes of the rhombohedral phase are at the frequencies close to the values in the orthorhombic phase. The latter possibility is ruled out as the frequencies of Raman modes in rhombohedral phase (to be discussed latter) are not close to the above three modes. In rhombohedral phase at 7.4 GPa, A_g^2 and B_{2g} modes soften anomalously (the effect is more for B_{2g} mode). Further Fig. 5 shows that the Raman modes N1, N2 and N3 show anomalous softening with pressure in rhombohedral as well as in simple cubic phase. It is clear from Fig. 5 that the slope S for the N3 mode is more than N1 and N2 modes. Fig. 6(a) shows the effect of pressure on FWHM of the Raman modes. The range from 0 to 4 GPa has been magnified in Fig. 6(b). The solid blue lines are the linear fit. It

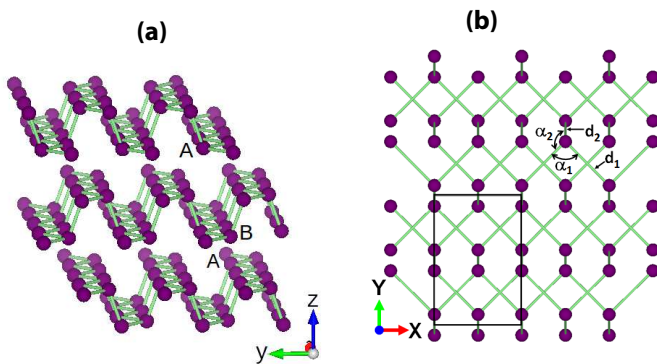


FIG. 1. Side (a) and top (b) views of the layered structure of bulk black phosphorus. d_1 and d_2 are the P-P bonds lengths. d_1 is the distance between two P atoms in a plane while d_2 is the nearest neighbor distance. α_1 is the bond angle between two d_1 's and the bond angle between d_1 and d_2 is α_2 .

is clear from Fig. 6(b) that the FWHM of all the three Raman modes show a minimum at 1.1 GPa which coincide with the ETT transition pressure. Another thing to note is that the line width of N1, N2 and N3 modes are very large. We don't fully understand the origin of the large linewidths of these modes in the rhombohedral phase. One possible origin could be the high disorder in the rhombohedral phase. We now present our theoretical calculations to understand the anomalies in phonon spectra with pressure observed in the experiments.

B. Theoretical calculations

1. Low Pressure Transition

BP is a semiconductor with a gap of 0.40 eV at Z-point (0.0, 0.0, 0.5) as estimated with HSE functional (Fig. 7(a)), which is in good agreement with the experiment ($E_g = 0.35$ eV). We note that there is no band gap in the structure at 0 GPa calculated with GGA functional based theory (Fig. 7(b)). Raman experiments (Fig. 6(b)) showed non-monotonic dependence of FWHM of A_g^1 , B_{2g} and A_g^2 modes on pressure, displaying a minimum at 1.1 GPa. Since the anomalous change in FWHM can be an indicator of electronic topological transition (ETT)³², and given the experimental observations of Xiang *et al.*³¹ and theoretical study of Gong *et al.*³⁰, we first studied electronic structure of black phosphorus as a function of hydrostatic pressure using highly accurate HSE calculations. Our calculations show that the band inversion occurs at Z point at $P_{c1} \sim 1.2$ GPa (Fig. 8) following which the band gap opens up above $P_{c1} \geq 1.2$ GPa (Fig. 7(c)), which is in contrast to the earlier DFT study (within GGA and mBJ functional) where persistence of robust band crossing is reported after band inversion³⁰. In an electronic topological transition the bandgap decreases with increasing pressure, closes at P_c and then increases

(opens up) with further increase in pressure³². We have plotted the bandgap of BP at Z-point (the point at which band inversion occurs) in the vicinity of critical pressure, which clearly shows bandgap reduces and then increases as a function of volume (Fig 2(b)) *i.e.*, the bandgap exhibits a minimum value at P_{c1} and then increases. This is associated with closure of bandgap at a k-point near Z-point. To probe this, we have used Wannier functions to interpolate and plot HSE band structure. Oscillating behavior in the bandgap along Z-M and Z- Γ is due to errors in interpolation of bands with Wannier functions near the gap closure point, where band energies are non-analytic functions of k. We find that the HSE bandgap minimum is at volume lower than of the equilibrium structure. Hence ETT occurs at positive pressure ($P_{c1} \sim 1.2$ GPa), which is comparable with the pressure of anomalies seen in experiments. Based on the HSE calculations, our estimate of the transition pressure is $P_{c1} \sim 1.2$ GPa, in reasonable agreement with theoretically predicted transition pressure (0.6 GPa) by Ruixiang *et al.*⁴⁹, and also close to the pressure of observed Raman anomalies ($P_{c1} \sim 1.1$ GPa).

Although earlier studies^{30,31} reported pressure induced electronic topological transition (Lifshitz transition) in black phosphorus following band inversion near $P = 1.2$ GPa, the nature of electronic topology has not been clearly elucidated. To investigate the electronic topology of black phosphorus, we determined the Z_2 topological invariant (ν_0) as a function of pressure (Fig. 9). The evolution of hybrid Wannier charge centers (WCCs) along k_y -direction is marked by circle while their largest gap function is marked by blue rhombus for $k_z = 0$ plane and $k_z = 0.5$ plane. It is clear from Fig. 9 (a),(b) that for $P < 1.2$ GPa both $k_z = 0$ and $k_z = 0.5$ planes are topologically trivial as Z_2 invariants for both the planes are zero, and hence strong topological index $\nu_0 = 0$. However, at $P > 1.2$ GPa (Fig. 9 (c),(d)), Z_2 invariant for $k_z = 0$ plane is 1, as evident from the discontinuous jump of the gap function along k_y , whereas Z_2 invariant is zero for $k_z = 0.5$ plane, and hence the strong topological index ν_0 of the state at this pressure is 1. Thus we find that $\nu_0 = 0$ for $P < 1.2$ GPa, whereas $\nu_0 = 1$ for $P \geq 1.2$ GPa signifying Z_2 topological insulating nature of black phosphorus above 1.2 GPa. Thus, the minimum in FWHM of Raman active modes at (P_{c1}) is correlated with the pressure induced electronic topological phase transition. The observation of non-trivial π Berry phase and colossal magneto-resistance for $P > 1.2$ GPa in experiment³¹ are also consistent with our finding that the BP becomes topologically non-trivial for $P > 1.2$ GPa. The discrepancy between our calculated transition pressure (1.2 GPa) and previously reported ones⁴⁹ (0.6 GPa) falls within the typical errors of DFT calculations.

Calculations of phonon frequencies and electron-phonon coupling are not straight-forward with the HSE functionals because (i) DFT-LR (DFT linear response) implementation with HSE functional is not available presently and (ii) frozen phonon method with fine mesh

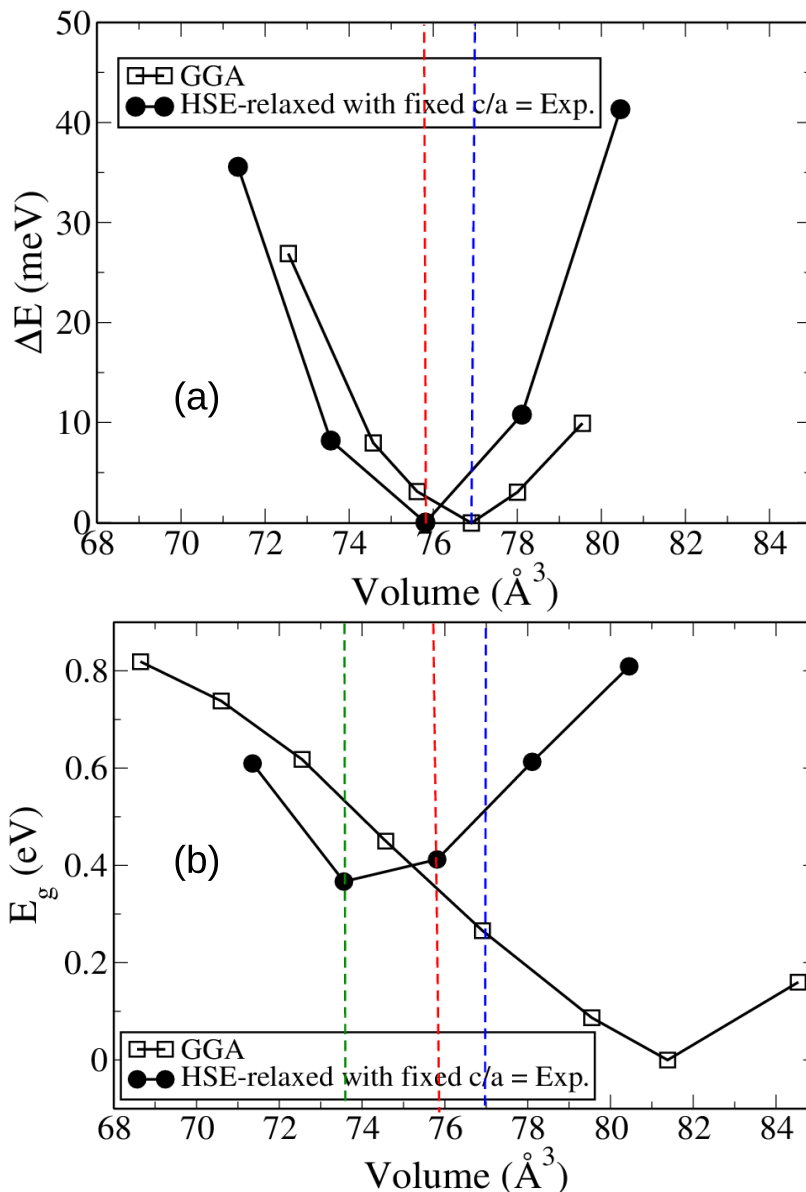


FIG. 2. Change in energy (a) and bandgap at Z-point of Brillouin zone (b) with volume obtained from calculations with GGA and HSE functionals. Red and blue dashed lines mark the equilibrium structure of BP in orthorhombic phase. Note that green dashed line highlights the volume at which bandgap of HSE-relaxed structure exhibits a minimum, making the electronic topological transition.

of k-points make HSE calculation very computationally intensive. Thus we have used GGA functional in understanding the observed phonon anomalies. We correct the pressures estimated in GGA calculations with a shift of 2.7 GPa, to match the transition pressure estimated with HSE calculations in the orthorhombic phase. Our optimized structural parameters of orthorhombic structure, a , b , c , d_1 , d_2 , α_1 and α_2 are 4.42 \AA , 3.32 \AA , 10.46 \AA , 2.224 \AA , 2.244 \AA , 96.34 $^\circ$ and 102.09 $^\circ$ respectively, in good agreement with the experimental⁵⁰ and earlier reported theoretical⁵¹ values. Here d_1 is the bond length of in-plane P atoms, d_2 defines the distance out-of-plane P atoms; α_2 and α_1 are the bond angles between d_1 and

d_2 , and the two d_1 bonds respectively (see Fig. 1(b)). Our calculated frequencies of A_g^2 , B_{2g} and A_g^1 modes using GGA functionals are 453 cm^{-1} , 424 cm^{-1} and 354 cm^{-1} , which agree well with the observed frequencies (460 cm^{-1} , 438 cm^{-1} and 360 cm^{-1}) of these modes.

We now examine the minimum in the FWHM (at P_{c1}) which is related to the electron phonon coupling constant λ . The dependence of λ of the three Raman modes on pressure shows a dip at -1.5 GPa. We have gone to negative pressure because GGA calculations show semiconductor to semi-metal transition at $P_{c1} = -1.5$ GPa. The discrepancy in P_{c1} using GGA functionals as compared

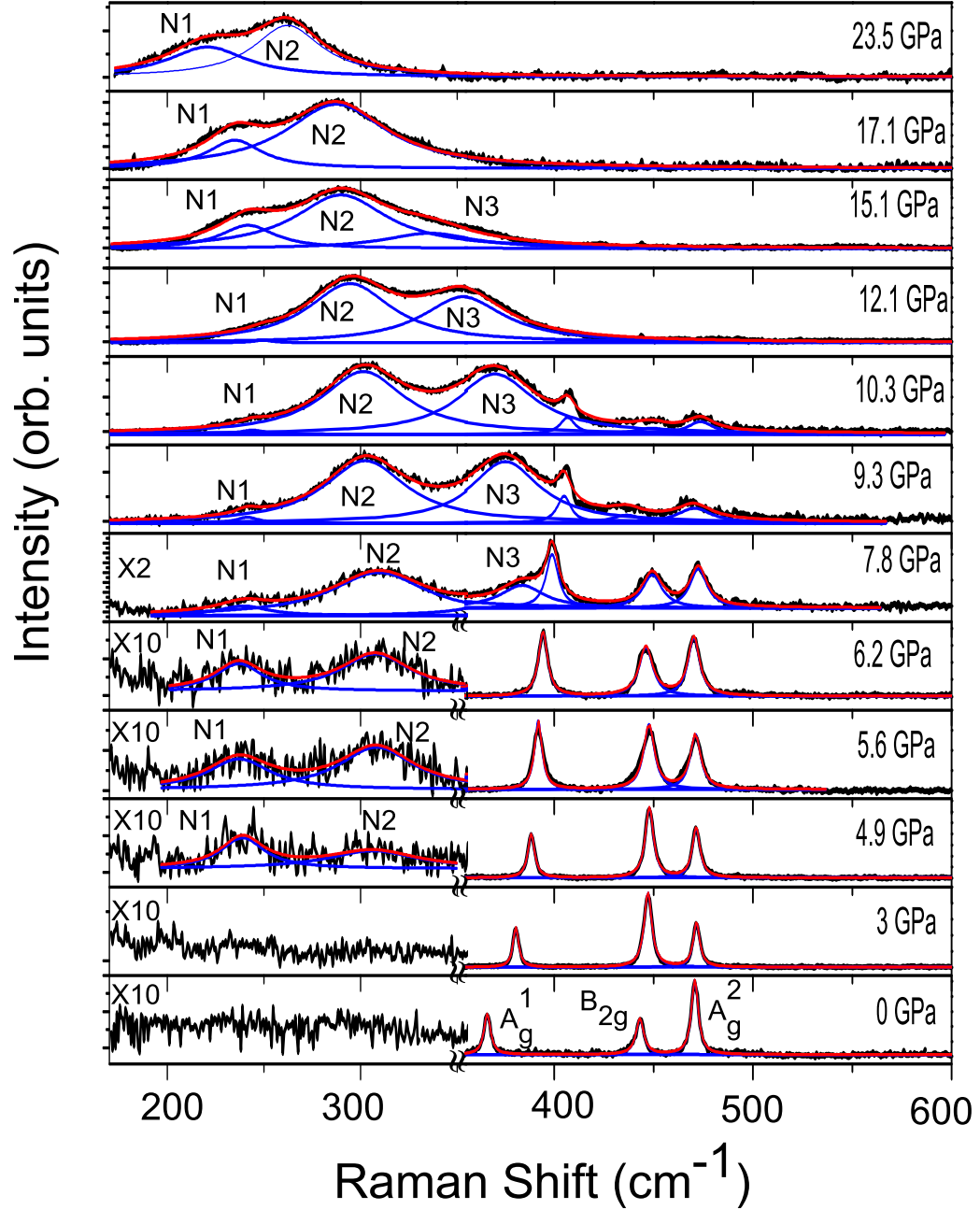


FIG. 3. Pressure evolution of Raman spectra. The solid lines (red and blue) are the Lorentzian fits to the experimental data (black). N1, N2 and N3 are the new modes.

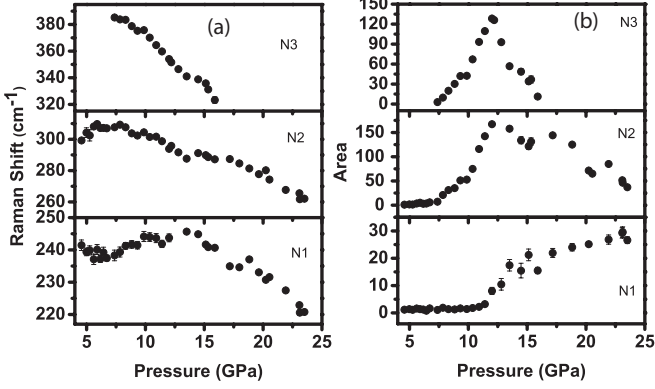


FIG. 4. Pressure dependence of phonon frequencies and area of N1, N2 and N3 modes.

to experiment ($P_{c1} = 1.1$ GPa) and HSE functionals ($P_{c1} = 1.2$ GPa) points to the inadequacy of the GGA functionals in estimation of bandgap and predicting the transition pressure. The corrected transition pressure will be $P_{c1}^{corrected} = -1.5 + 2.7 = 1.2$ GPa as indicated in Fig. 7(d). This correction is used in the pressure axis in plotting Fig. 6 (c). Further, with increasing pressure, the gap closes in the vicinity of Z-point at $P^{corrected} = 1.7$ GPa (Fig. 7(d)). Fig. 6 (c) reveals that the λ does show a shallow minimum at $P_{c1}^{corrected} = 1.2$ GPa for the A_g^1 and A_g^2 modes. clearly establishing the link between a dip in λ and FWHM with the ETT. We did not see any anomaly in the λ of B_{2g} mode with pressure.

The linewidth of a phonon mode of a crystal exhibiting a strong electron-phonon interaction is largely determined by electron-phonon coupling (EPC). The relation between the EPC ($\lambda_{q\nu}$) and FWHM ($\gamma_{q\nu}$)^{52,53} of a phonon ν at wavevector q is given by the following expression,

$$\lambda_{q\nu} = \frac{\gamma_{q\nu}}{\pi \hbar N(\epsilon_F) \omega_{q\nu}^2}, \quad (2)$$

where $N(\epsilon_F)$ is the density of electronic states at Fermi level. From Eq. (2), it is clear that λ and FWHM are proportional to each other. Since the density of states and electronic bands involved in the matrix elements $\gamma_{q\nu}$ change upon band inversion at the ETT, there is thus a causal relationship with anomaly in FWHM. Hence, we see a minimum in FWHM and λ of a mode at the transition pressure. The anomalous change in observed FWHM may not in general indicate an electronic topological transition (ETT). In the present context, however, a careful analysis of calculated electronic structure of black phosphorous reveals a band inversion across the transition pressure (~ 1.2 GPa), indicating the occurrence of an ETT. Our calculations of Z_2 invariant across $P_{c1} \sim 1.2$ GPa confirm this topological transition from trivial semiconductor to topological semimetallic state. ETT is accompanied by the Lifshitz transition, the electronic structure changes and the charge density of P

atoms redistributes, leading to the anomaly of Raman spectra.

2. Anomalies at High Pressure Transitions: Structural Origin

We now address the pressure dependence of phonon frequencies of A_g^1 , A_g^2 and B_{2g} modes of the orthorhombic phase. The calculated frequencies of the orthorhombic phase as a function of pressure (Fig. 10) clearly display that the frequencies of A_g^1 and A_g^2 modes harden up to ~ 5 GPa. Interestingly, the frequency of B_{2g} and A_g^2 modes show softening at high pressure; resembling with the anomalous pressure dependence of the B_{2g} and A_g^2 modes seen in the experiments between 7 and 9 GPa (Fig. 5). To correlate the softening of the B_{2g} and A_g^2 modes with structural modifications, we examine the pressure dependence of the internal parameters d_1 , d_2 , α_1 and α_2 (see Fig. 1 for description).

Atomic vibrations of the A_g^1 mode (Fig. 10) involve stretching of the d_2 bond. From the variation in d_2 bond with pressure (Fig. 11(a)), we find that d_2 decreases monotonically with pressure and the Δd_2 is ~ 0.04 Å up to 14.7 GPa. As a result, A_g^1 hardens with pressure. The atomic vibrations of the B_{2g} mode (Fig. 10) affects bond angle α_2 , which decreases with increasing pressure (Fig. 11(b)), similar to the frequency of B_{2g} mode. Atomic displacements of the A_g^2 mode (Fig. 10) involve stretching of the d_1 bond. Fig. 11(a) shows that d_1 decreases with pressure upto 6 GPa, and starts increasing from 7-11 GPa, and subsequently decreases with pressure upto 14.7 GPa. In this case, the change in d_1 with pressure is much smaller than that in d_2 , which is also reflected in softening of B_{2g} and A_g^2 modes. As a result of variation of d_1 with pressure, the A_g^2 mode softens with pressure and this softening is less than the softening of the B_{2g} mode. The pressure axes of Fig. 10 and Fig. 11 are corrected with a shift of +2.7 GPa as described in the previous section. Our theoretical calculations reveal that black phosphorous is quite a soft material, with its cell volume at 14.7 GPa being 24% smaller than that at 0 GPa. This large change in volume with pressure is responsible for significant softening of B_{2g} and A_g^2 modes. For such large changes in volume, we expect anharmonic effects to be strong, which are not included in our analysis. This is probably responsible for some discrepancy between theory and experiments. We find that the observed softening of A_g^2 mode (Fig. 10) is not indefinite: A_g^2 mode harden with further increase in pressure beyond 15 GPa, consistent with our experiments.

Orthorhombic phase is a low pressure phase of black phosphorous which is stable only at $P < 5$ GPa. We presented results of our calculations on orthorhombic phase at $P > 5$ GPa because experiments are indicative of the presence of mixed phases at higher pressure, as evidenced in the survival of A_g^1 , B_{2g} and A_g^2 modes at high pressures along with the modes N1 (E_g), N2 (A_{1g}) and N3

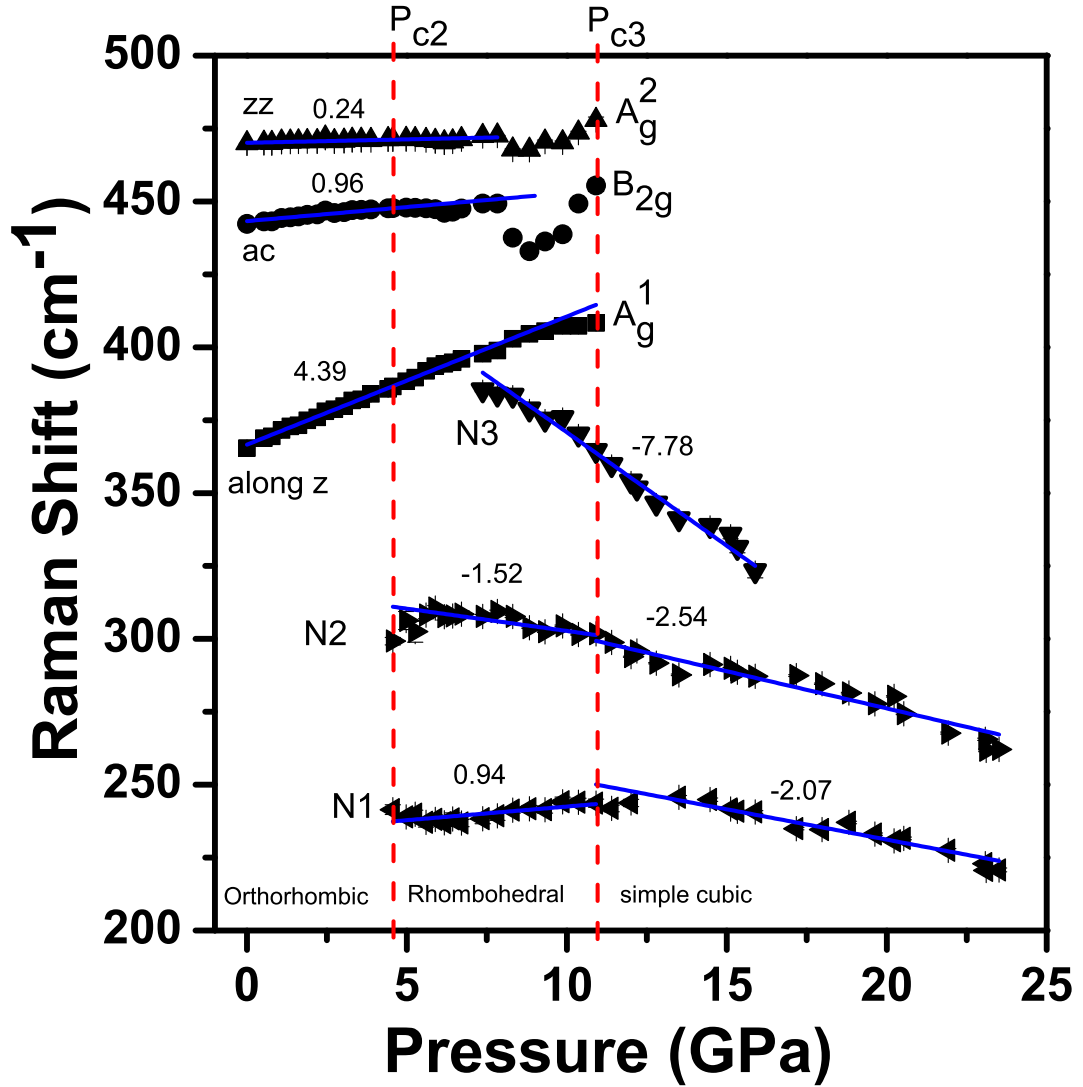


FIG. 5. Pressure dependence of phonon frequencies. The vertical dashed lines indicate the two structural phase transition pressures. The solid blue lines are the linear fit. The slope $d\omega/dP$ in units of $\text{cm}^{-1}/\text{GPa}$ is given near the lines.

(E_g) of the rhombohedral phase (refer Fig. 5). As the calculations here are on pure and not on mixed phases (orthorhombic and rhombohedral phases together as seen in experiment), interpretation of experimental and theoretical results should be done with care.

The space group of BP in rhombohedral structure (also known as A7 phase after 4.6 GPa) is $R\bar{3}m$ with primitive cell containing 2 atoms. Group theory gives zone center optical modes as $A_{1g} + E_g + A_{2u} + E_u$, where A_{1g} and E_g are the Raman active modes and A_{2u} and E_u are infrared active modes. We used hexagonal unit cell with 6 atoms (*i.e.* a supercell) to perform phonon calculations for A7 phase. Some of the zone boundary points of BZ of rhom-

bohedral structure (*i.e.* the primitive cell) fold onto the Γ -point of BZ of the hexagonal unit cell, and enable the analysis of Raman active modes and their symmetries. The frequencies of the Raman active modes E_g^2 , A_{1g} and E_g^1 modes are 367 cm^{-1} , 336 cm^{-1} and 242 cm^{-1} respectively at 4 GPa. Calculated frequencies of these modes are in good agreement with experimental values (*e.g.* at 6 GPa, ω (N1) = 237 cm^{-1} (Exp. 237 cm^{-1}), ω (N2) = 311 cm^{-1} (Exp. 307 cm^{-1})). We identify the experimentally observed N3 mode as E_g^2 , N2 mode as A_{1g} mode and N1 mode as E_g^1 . Symmetry assignment of N2 and N1 modes is consistent with previous report²². All the three modes N1, N2 and N3 soften with pressure, in agreement with

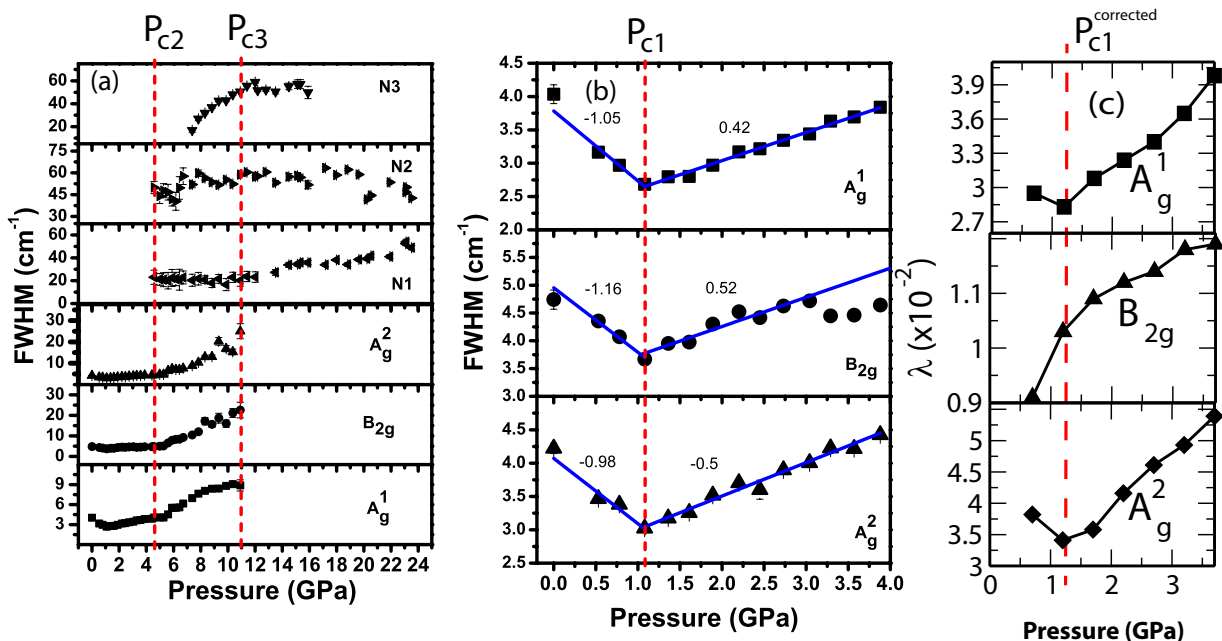


FIG. 6. (a) Pressure evolution of FWHM of Raman modes. The vertical dashed lines indicate the two structural phase transition pressures. (b) Magnified plot FWHM in the pressure range 0 to 4 GPa. The vertical dashed line indicates the semiconductor to topological insulator phase transition pressures. The solid blue lines are linear fit. The slope $d\omega/dP$ in units of $\text{cm}^{-1}/\text{GPa}$ is given near the lines. (c) Variation in the calculated electron-phonon coupling of Raman active modes A_g^1 , B_{2g} and A_g^2 of BP with pressure in orthorhombic phase calculated using GGA functional. The pressure axis has been corrected as explained in the text. The vertical dashed line indicates the semiconductor to topological insulator phase transition pressures.

the observed trends in our experiment (see Fig. 12 and Fig. 5). From first-principles calculations, we find that the A7-phase (hexagonal structure) is stable at pressures from 4 GPa to 12 GPa and, as unstable modes appear in phonon dispersion beyond this pressure. The N1 and N2 modes also persist at pressures till 24 GPa (sc phase). It is likely that the A7-phase exists beyond 11 GPa. There are no Raman active modes in the sc phase with one atom per unit cell. Another possibility is that the modes N1 and N2 are the disorder activated zone boundary acoustic phonons of the sc phase. To examine this possibility, we carried out calculations of the zone boundary acoustic phonons of the sc phase. Our calculations indeed show acoustic modes at X point (283 cm^{-1}) and M point (340 cm^{-1}), which exhibit the pressure dependence similar to that of N1 and N2 modes *i.e* both of them soften with pressure (Fig. 12). Thus, we have assigned N1 and N2 modes in the sc phase to these zone boundary acoustic modes.

V. CONCLUSION

High pressure Raman study of BP up to 24 GPa is reported using diamond anvil cell under hydrostatic conditions. The line width of all the three Raman modes A_g^1 , B_{2g} and A_g^2 of the orthorhombic phase decrease with pressure up to 1.1 GPa and then increase, thus showing a minimum at ~ 1.1 GPa corresponding to the transition pres-

sure of ETT. Using first-principles calculations, we find that the low pressure phase transition in BP is a semiconductor to topological insulator transition. Our calculations of the Z_2 invariant confirm the change in electronic topology marking a transition from band to topological insulating state. The Raman shift of these modes show normal hardening with pressure in orthorhombic phase. B_{2g} and A_g^2 modes show anomalous softening in rhombohedral phase at 7.4 GPa while A_g^1 mode exhibits normal hardening. These modes disappear completely at 11 GPa in the sc phase. The new modes N1, N2 and N3 arising in rhombohedral phase also show anomalous softening of the frequency with pressure. We uncover the origin of these anomalous softening of Raman modes in the variation of internal structural parameters with pressure, and identify the symmetry of the new modes appearing upon pressure in experiments.

VI. ACKNOWLEDGEMENTS

AS is grateful to Jawaharlal Nehru Centre for Scientific Advanced Research, India for research fellowship. AKS and UVW thank DST for the JC Bose National fellowships. AKS thanks DST Nanomission for the financial support.

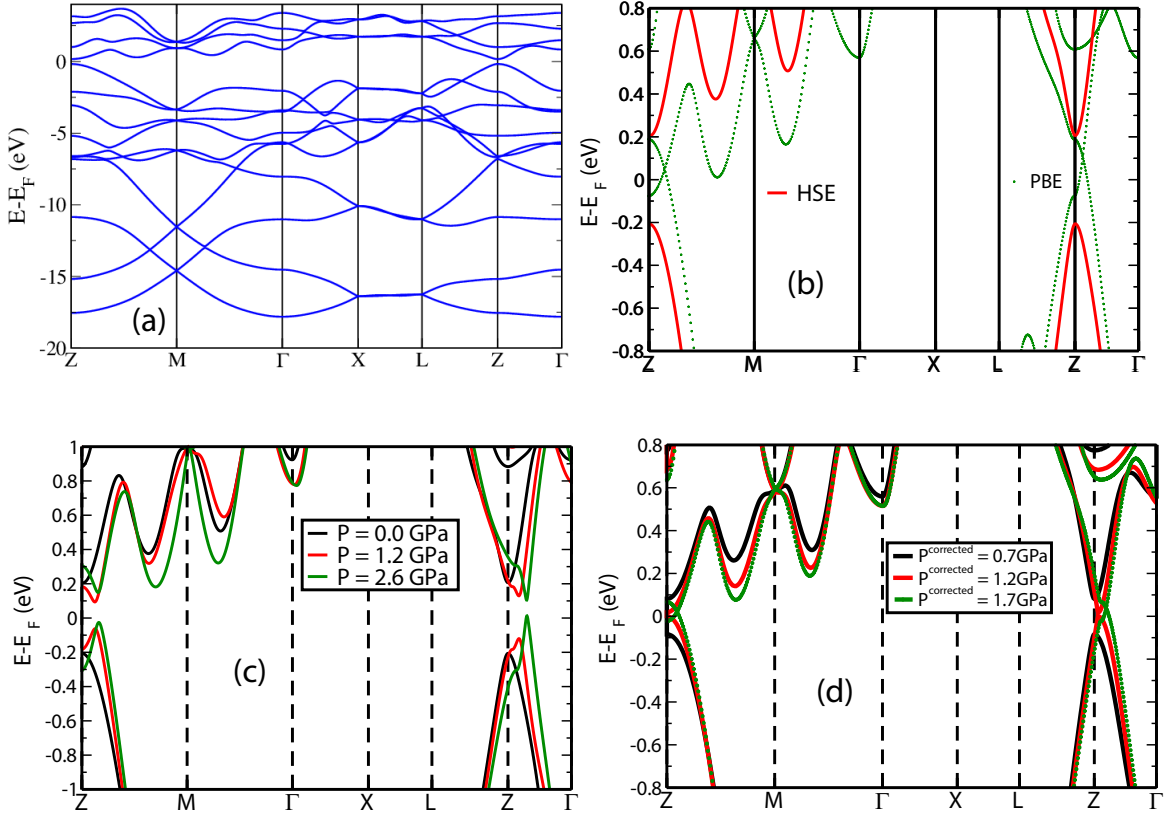


FIG. 7. Electronic structure of BP in orthorhombic phase. (a) Electronic structure of BP at $P = 0$ GPa calculated with HSE functionals. Note that we used Wannier functions⁵⁴ to plot band structure with HSE functionals. (b) Comparison of electronic structure near the gap obtained with HSE and PBE functionals at $P = 0$ GPa. BP exhibits a gap of 0.33 eV at Z-point, which is captured correctly with HSE functionals whereas PBE calculations gives no gap. (c) Electronic structure near the gap obtained with HSE functionals at different pressures. (d) Electronic structure of BP calculated with PBE-GGA functional at different pressures. The pressures have been corrected as explained in the text. At $p^{\text{corrected}} = 0.7$ GPa, calculations with PBE functionals show a gap which closes at $p^{\text{corrected}} = 1.2$ GPa. With further increase in pressure, bandgap closes in vicinity of Z-point at $p^{\text{corrected}} = 1.7$ GPa.

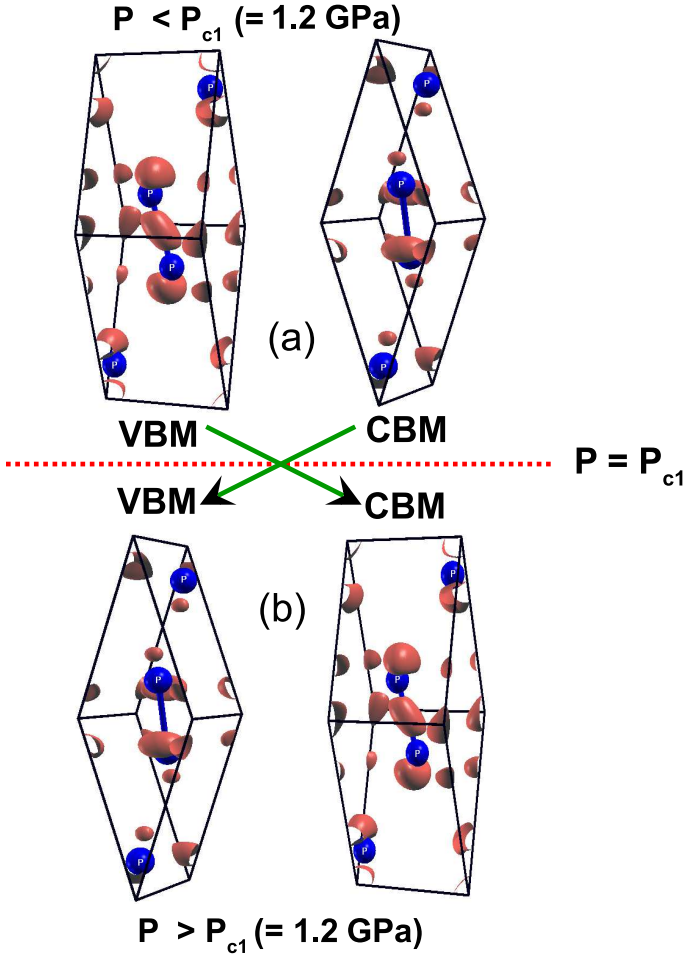


FIG. 8. Band inversion during pressure induced electronic topological transition (ETT) in BP. Isosurfaces of charge densities associated with electronic states at valence band maximum (VBM) and conduction band minimum (CBM) at Γ -point (a) before and (b) after the ETT revealing band inversion across this transition.

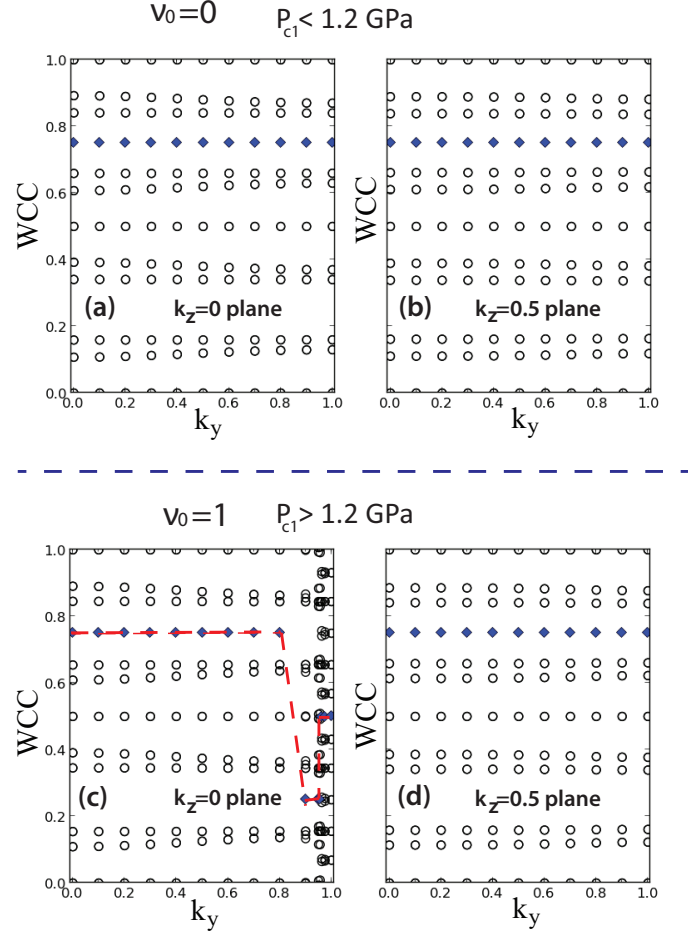


FIG. 9. Calculation of Z_2 topological index (ν_0) before ($P < 1.2 \text{ GPa}$) and after ($P > 1.2 \text{ GPa}$) the phase transition. Evolution of hybrid Wannier charge centers (WCCs) along k_y -direction (marked by circle) and their largest gap function (blue rhombus) for (a) $k_z = 0$ plane and (b) $k_z = 0.5$ plane. It is clear that both $k_z = 0$ and $k_z = 0.5$ planes are topologically trivial as Z_2 invariants for both the planes are zero, hence strong topological index $\nu_0 = 0$. At $P > 1.2 \text{ GPa}$, Z_2 invariant for $k_z = 0$ plane is 1, as evident from the discontinuous jump (indicated by red dotted line) of the gap function along k_y (c), whereas Z_2 invariant is zero for $k_z = 0.5$ plane (d), hence the strong topological index ν_0 at this pressure is 1.

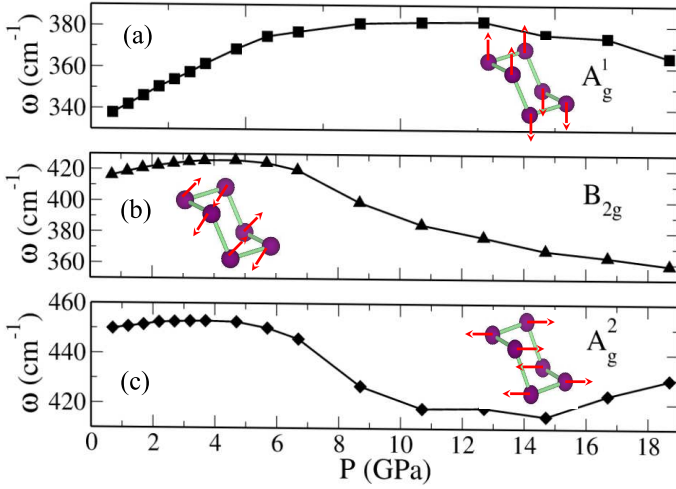


FIG. 10. Change in the calculated frequencies of Raman active modes (a) A_{1g}^1 , (b) B_{2g} and (c) A_{2g}^2 modes of BP in orthorhombic phase with pressure. Insets of (a), (b) and (c) show atomic displacements in these Raman active modes. The pressure axis has been corrected as explained in the text.

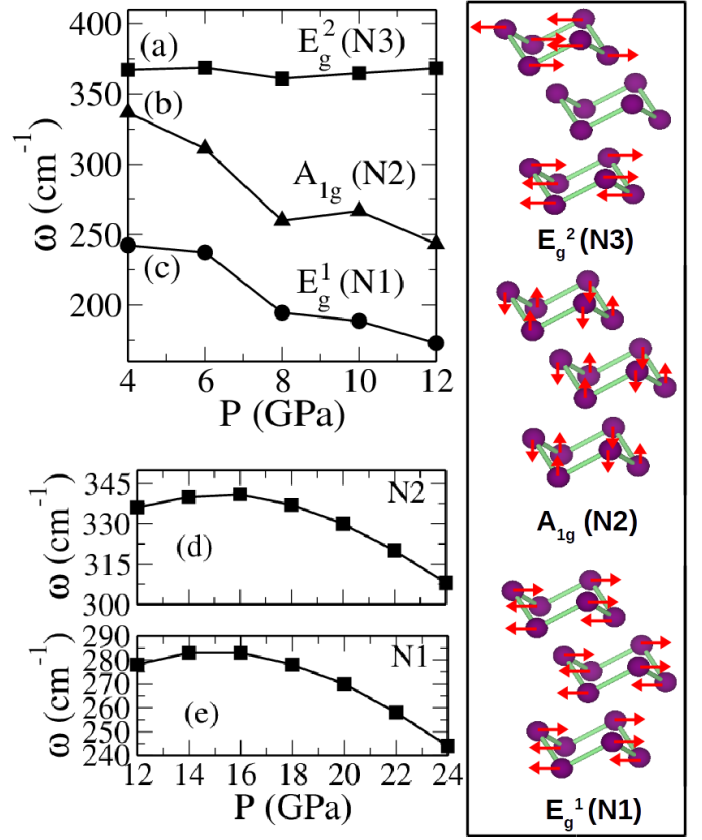


FIG. 12. Changes in the calculated frequencies of Raman active modes of BP, (a) E_g^2 (N3), (b) A_{1g} (N2) and (c) E_g^1 (N1) modes in rhombohedral phase (right panel shows their atomic displacements) with pressure, (d) N2 and (e) N1 modes with pressure of BP in cubic phase. Note that N1, N2 and N3 are the modes observed in experiments. N2 and N1 modes as shown in figure (d) and (e) correspond to the acoustic modes at X and M-points in the Brillouin Zone of the simple cubic phase.

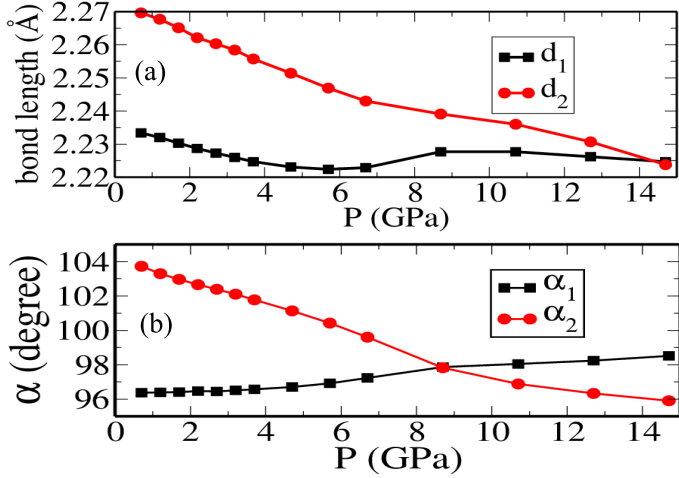


FIG. 11. Evolution of bond lengths (a) and bond angles (b) of BP in orthorhombic phase with pressure. The pressure axis has been corrected as explained in the text.

- * To whom correspondence should be addressed; asood@physics.iisc.ernet.in
- ¹ X. Ling, H. Wang, S. Huang, F. Xia, and M. S. Dresselhaus, *Proc. Natl. Acad. Sci.* **112**, 4523 (2015).
 - ² B. Chakraborty, S. N. Gupta, A. Singh, M. Kuiri, C. Kumar, D. Muthu, A. Das, U. Waghmare, and A. Sood, *2D Materials* **3**, 015008 (2016).
 - ³ L. Li, Y. Yu, G. J. Ye, Q. Ge, X. Ou, H. Wu, D. Feng, X. H. Chen, and Y. Zhang, *Nat. Nanotechnol.* **9**, 372 (2014).
 - ⁴ F. Xia, H. Wang, and Y. Jia, *Nature commun.* **5**, 4458 (2014).
 - ⁵ H. Liu, A. T. Neal, Z. Zhu, Z. Luo, X. Xu, D. Tománek, and P. D. Ye, *ACS Nano* **8**, 4033 (2014).
 - ⁶ S. P. Koenig, R. A. Doganov, H. Schmidt, A. C. Neto, and B. Oezylmaz, *App. Phys. Lett.* **104**, 103106 (2014).
 - ⁷ A. Rodin, A. Carvalho, and A. C. Neto, *Phys. Rev. Lett.* **112**, 176801 (2014).
 - ⁸ J. Qiao, X. Kong, Z.-X. Hu, F. Yang, and W. Ji, *Nature Commun.* **5**, 4475 (2014).
 - ⁹ S. Zhang, J. Yang, R. Xu, F. Wang, W. Li, M. Ghufuran, Y.-W. Zhang, Z. Yu, G. Zhang, Q. Qin, et al., *ACS Nano* **8**, 9590 (2014).
 - ¹⁰ K. Novoselov, A. K. Geim, S. Morozov, D. Jiang, M. Katsnelson, I. Grigorieva, S. Dubonos, and A. Firsov, *Nature* **438**, 197 (2005).
 - ¹¹ Y. Zhang, Y.-W. Tan, H. L. Stormer, and P. Kim, *Nature* **438**, 201 (2005).
 - ¹² K. F. Mak, C. Lee, J. Hone, J. Shan, and T. F. Heinz, *Phys. Rev. Lett.* **105**, 136805 (2010).
 - ¹³ A. Splendiani, L. Sun, Y. Zhang, T. Li, J. Kim, C.-Y. Chim, G. Galli, and F. Wang, *Nano Lett.* **10**, 1271 (2010).
 - ¹⁴ A. M. Jones, H. Yu, J. S. Ross, P. Klement, N. J. Ghimire, J. Yan, D. G. Mandrus, W. Yao, and X. Xu, *Nature Phys.* **10**, 130 (2014).
 - ¹⁵ H. Liu, Y. Du, Y. Deng, and D. Y. Peide, *Chem. Soc. Rev.* **44**, 2732 (2015).
 - ¹⁶ J. C. Jamieson, *Science* **139**, 1291 (1963).
 - ¹⁷ L. Cartz, S. Srinivasa, R. Riedner, J. Jorgensen, and T. Worlton, *J. Chem. Phys.* **71**, 1718 (1979).
 - ¹⁸ T. Kikegawa and H. Iwasaki, *Acta Crystallogr. Sect. B* **39**, 158 (1983).
 - ¹⁹ J. K. Burdett and S. Lee, *J. Solid State Chem.* **44**, 415 (1982).
 - ²⁰ S. Sugai, T. Ueda, and K. Murase, *J. Phys. Soc. Jpn.* **50**, 3356 (1981).
 - ²¹ C. Vanderborgh and D. Schiferl, *Phys. Rev. B* **40**, 9595 (1989).
 - ²² Y. Akahama, M. Kobayashi, and H. Kawamura, *Solid State Commun.* **104**, 311 (1997).
 - ²³ Y. Akahama, M. Kobayashi, and H. Kawamura, *Phys. Rev. B* **59**, 8520 (1999).
 - ²⁴ Y. Akahama, H. Kawamura, S. Carlson, T. Le Bihan, and D. Häusermann, *Phys. Rev. B* **61**, 3139 (2000).
 - ²⁵ J. Wittig and B. Matthias, *Science* **160**, 994 (1968).
 - ²⁶ H. Kawamura, I. Shirovani, and K. Tachikawa, *Solid state commun.* **49**, 879 (1984).
 - ²⁷ Y. Akahama and H. Kawamura, *Phys. Status Solidi B* **223**, 349 (2001).
 - ²⁸ M. Okajima, S. Endo, Y. Akahama and S. Narita, *Jpn. J. Appl. Phys.* **23**, 15, (1984).
 - ²⁹ Y. Akahama, S. Endo, and S. Narita, *Physica B+ C* **139**, 397 (1986).
 - ³⁰ P.-L. Gong, D.-Y. Liu, K.-S. Yan, Z.-J. Xiang, X.-H. Chen, S.-Q. Shen, and L.-J. Zou, *Phys. Rev. B* **93**, 195434 (2016).
 - ³¹ Z. J. Xiang, G. J. Ye, C. Shang, B. Lei, N. Z. Wang, K. S. Yang, D. Y. Liu, F. B. Meng, X. G. Luo, L. J. Zou, et al., *Phys. Rev. Lett.* **115**, 186403 (2015).
 - ³² A. Bera, K. Pal, D. V. S. Muthu, S. Sen, P. Guptasarma, U. V. Waghmare, and A. K. Sood, *Phys. Rev. Lett.* **110**, 107401 (2013).
 - ³³ K. Pal and U. V. Waghmare, *Appl. Phys. Lett.* **105**, 062105 (2014).
 - ³⁴ X. Xi, C. Ma, Z. Liu, Z. Chen, W. Ku, H. Berger, C. Martin, D. B. Tanner, and G. L. Carr, *Phys. Rev. Lett.* **111**, 155701 (2013).
 - ³⁵ A. Manjanath, A. Samanta, T. Pandey and A. K. Singh, *Nanotechnology*, **26**, 075701, (2015).
 - ³⁶ K. Akiba, A. Miyake and Y. Akahama, K. Matsubayashi, Y. Uwatoko, H. Arai, Y. Fuseya and M. Tokunaga, *J. Phys. Soc. Jpn.* **84**, 073708, (2015).
 - ³⁷ Y. Yamada, Y. Fujii, Y. Akahama, S. Endo, S. Narita, J. D. Axe, and D. B. McWhan, *Phys. Rev. B* **30**, 2410 (1984).
 - ³⁸ T. Sasaki, K. Kondo, Y. Akahama, S. Nakano, and T. Taniguchi, *Jpn. J. Appl. Phys.* **56**, 05FB06 (2017).
 - ³⁹ P. Giannozzi, S. Baroni, N. Bonini, M. Calandra, R. Car, C. Cavazzoni, D. Ceresoli, G. L. Chiarotti, M. Cococcioni, I. Dabo, et al., *J. Phys. Condens. Matter* **21**, 395502 (2009).
 - ⁴⁰ S. Goedecker, M. Teter, and J. Hutter, *Phys. Rev. B* **54**, 1703 (1996).
 - ⁴¹ C. Hartwigsen, S. Goedecker, and J. Hutter, *Phys. Rev. B* **58**, 3641 (1998).
 - ⁴² J. P. Perdew, K. Burke, and M. Ernzerhof, *Phys. Rev. Lett.* **77**, 3865 (1996).
 - ⁴³ S. Grimme, *J. Comput. Chem.* **25**, 1463 (2004).
 - ⁴⁴ J. Heyd, G. E. Scuseria, and M. Ernzerhof, *J. Chem. Phys.* **118**, 8207 (2003).
 - ⁴⁵ A. A. Soluyanov and D. Vanderbilt, *Phys. Rev. B* **83**, 235401 (2011).
 - ⁴⁶ J. Bhattacharjee and U. V. Waghmare, *Phys. Rev. B* **71**, 045106 (2005).
 - ⁴⁷ L. Fu and C. L. Kane, *Phys. Rev. B* **74**, 195312 (2006).
 - ⁴⁸ D. Gresch, O. Y. G. Autés, T. M. D. Vanderbilt, B. A. Bernevig, and A. A. Soluyanov, arXiv:1610.08983v1 (2016).
 - ⁴⁹ R. Fei, V. Tran, and L. Yang, *Phys. Rev. B* **91**, 195319 (2015).
 - ⁵⁰ T. Akai, S. Endo, Y. Akahama, K. Koto and Y. Maruyama, *High Press. Res.* **1**, 115 (1989).
 - ⁵¹ S. Appalakondaiah, G. Vaitheeswaran, S. Lebègue, N. E. Christensen, and A. Svane, *Phys. Rev. B* **86**, 035105, (2012).
 - ⁵² Simone Pisana, Michele Lazzeri, Cinzia Casiraghi, Kostya S. Novoselov, A. K. Geim, Andrea C. Ferrari and Francesco Mauri, *Nat. Mater.*, **6**, 198, (2007).
 - ⁵³ Michele Lazzeri, S. Piscanec, Francesco Mauri, A. C. Ferrari, and J. Robertson, *Phys. Rev. B*, **73**, 155426, (2006).
 - ⁵⁴ A. A. Mostofi, J. R. Yates, G. Pizzi, Y.-S. Lee, I. Souza, D. Vanderbilt, and N. Marzari, *Comput. Phys. Commun.* **185**, 2309 (2014).